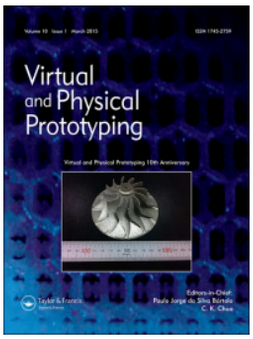

Taylor & Francis
Taylor & Francis Group

Virtual and Physical Prototyping

ISSN: 1745-2759 (Print) 1745-2767 (Online) Journal homepage: www.tandfonline.com/journals/nvpp20

Enhancing mechanical performance of elastomeric vat-photopolymerized resins via functionalized cellulose nanocrystals

Wonhee Lee, Eui-Hyuk Kim , Tim Kuehnel , Jinhong Min, Jiho Lee, Hoon Kim & Yong-Jin Yoon

To cite this article: Wonhee Lee, Eui-Hyuk Kim , Tim Kuehnel , Jinhong Min, Jiho Lee, Hoon Kim & Yong-Jin Yoon (2026) Enhancing mechanical performance of elastomeric vat-photopolymerized resins via functionalized cellulose nanocrystals, Virtual and Physical Prototyping, 21:1, e2662727, DOI: 10.1080/17452759.2026.2662727

To link to this article: https://doi.org/10.1080/17452759.2026.2662727

Published online: 06 May 2026.

VIRTUAL AND PHYSICAL PROTOTYPING
2026, VOL. 21, NO. 1, e2662727 (14 pages)
https://doi.org/10.1080/17452759.2026.2662727

Enhancing mechanical performance of elastomeric vat-photopolymerized resins via functionalized cellulose nanocrystals

Wonhee Lee [a], Eui-Hyuk Kim[a], Tim Kuehnel[a,b], Jinhong Min [c], Jiho Lee [c], Hoon Kim [c] and Yong-Jin Yoon [a,d,e]

[a]Department of Mechanical Engineering, Korea Advanced Institute of Science and Technology (KAIST), Daejeon, Republic of Korea; [b]Department of Mechanical Engineering, Karlsruhe Institute of Technology, Karlsruhe, Germany; [c]Department of Research Planning, Graphy R&D Center, Graphy Inc., Seoul, Republic of Korea; [d]School of Mechanical & Aerospace Engineering, Nanyang Technological University, Singapore, Singapore; [e]KAIST InnoCORE PRISM-AI Center, Korea Advanced Institute of Science and Technology (KAIST), Daejeon, Republic of Korea

ABSTRACT

Vat photopolymerization (VP) additive manufacturing enables precise, reproducible fabrication of complex biomedical devices, yet elastomeric resins with robust mechanics remain scarce for constrained surgical settings. Cellulose nanocrystals (CNC) are appealing reinforcements owing to high strength, biodegradability and biocompatibility, but their hydrophilicity limits compatibility with hydrophobic resins and drives agglomeration at higher loadings. Acrylated CNC (ACNC) was synthesised to increase hydrophobicity and promote interfacial bonding. Elastic resins with varied CNC or ACNC loadings were 3D printed by VP and characterised by tensile testing, transmission electron microscopy (TEM), Fourier transform infrared spectroscopy (FTIR) and rheology. Both fillers increased tensile strength, modulus, elongation and toughness relative to the neat resin, with the maximum improvement observed at 0.01 phr; ACNC consistently outperformed CNC. TEM showed relatively well-dispersed nanofillers at low concentration, whereas higher levels agglomerated and reduced reinforcement. FTIR and rheology indicated stronger covalent interactions and enhanced network formation in ACNC composites, yielding superior interfacial adhesion. Although interfacial bonding rose with filler level, agglomeration ultimately governed performance. These results demonstrate the feasibility of CNC-based nanofillers in VP elastomers and highlight ACNC as a sustainable route to high performance, patient-specific biomedical materials with clear practical relevance to constrained surgical environments.

ARTICLE HISTORY
Received 13 November 2025
Accepted 16 April 2026

KEYWORDS
Cellulose nanocrystals; 3D printing; elastomer; mechanical properties; agglomerations

1. Introduction

Additive manufacturing (AM), also referred to as three-dimensional (3D) printing, is a technique that fabricates 3D structures through a layer-by-layer deposition process [1]. This approach enables the production of complex geometries and has driven major advancements in materials and manufacturing technologies across diverse industrial sectors [2,3], with particularly broad applicability in the biomedical field [4–6]. Among various AM techniques, vat photopolymerization (VP) achieves the highest resolution and lowest surface roughness, making it especially suitable for fabricating patient-specific instruments (PSI) [7,8]. VP-manufactured PSI has been successfully applied in orthopedics with reproducible outcomes [9]. However, in laparoscopic or other spatially constrained surgical environments, softer elastomeric materials are required instead of rigid ones [10] and for applications involving soft tissue, materials with relatively low elastic modulus are essential [11]. The use of elastomeric materials in VP-based medical devices has been reported [12] and previous studies have investigated 3D printing techniques for highly stretchable materials with elastomer-like properties [13–16].

Cellulose nanocrystals (CNC), nanoparticles extracted from plants, have been widely utilised as additives due to their high mechanical strength, degradability and biocompatibility [17]. Their superior biocompatibility compared to other fillers makes CNC especially attractive for biomedical applications, and their use in 3D printing has recently gained attention [18]. Several studies have

CONTACT Yong-Jin Yoon yongjiny@kaist.ac.kr Department of Mechanical Engineering, Korea Advanced Institute of Science and Technology (KAIST), Daejeon 34141, Republic of Korea; School of Mechanical & Aerospace Engineering, Nanyang Technological University, 50 Nanyang Avenue, 639798, Singapore, Singapore KAIST InnoCORE PRISM-AI Center, Korea Advanced Institute of Science and Technology (KAIST), Daejeon 34141, Republic of Korea; Hoon Kim c12o2cl4@snu.ac.kr Department of Research Planning, Graphy R&D Center, Graphy Inc., Seoul, 08501, Republic of Korea

demonstrated that CNC incorporation enhances mechanical properties: Palaganas et al. reported a 100% increase in tensile strength, a rise in strain from 2% to 5%, and over a 200% increase in toughness when CNC were added to neat resin [19], while Abidnejad et al. observed improvements in tensile, three-point bending, and impact strength [20]. Despite these benefits, the hydrophilic nature of CNC limits compatibility with hydrophobic polymers and promotes agglomeration [21]. Rosa et al. showed that blending CNC with poly(ethylene glycol) diacrylate (PEGDA) enhanced mechanical properties but still led to agglomeration at concentrations as low as 0.6 wt% [22]. Furthermore, Maturi et al. reported deterioration of mechanical performance when CNC were directly integrated into hydrophobic resins without proper surface treatment [23].

To address the limitations of CNC agglomeration and poor compatibility with hydrophobic matrices, various strategies have been explored, including modifying the hydrophobicity of the base matrix and chemically functionalising the CNC surface. Li et al. mitigated agglomeration by pre-reacting CNC with the hydrophilic monomer 1,3-diglycerolate diacrylate (DiGlyDA) prior to blending with PEGDA, which improved dispersion and mechanical properties [24]. Maturi et al. enhanced CNC hydrophobicity through surface modification with acrylated epoxidized soybean oil [23]. Other studies have similarly developed modified CNC for 3D printing applications, demonstrating improved resin compatibility, better dispersion and enhanced mechanical performance [21,25,26]. More recently, advanced matrix systems such as shape memory polymers have been combined with CNC or modified CNC to further expand material functionality [25]. Despite these advances, the integration of CNC into soft elastomeric systems for VP-based 3D printing remains largely unexplored. Although CNC–elastomer composites have been reported [27], fabrication was achieved through mollding rather than 3D printing. Moreover, efforts to incorporate functionalised CNC into epoxy resins for 3D printing yielded only modest improvements in mechanical properties [28]. While surface modification of CNC has been explored in several photocurable resin systems, previous studies have primarily focused on dielectric or bio-based shape-memory materials [29,30]. In contrast, the present study investigates the incorporation of CNC and acrylated CNC into a soft elastomeric VP-printable resin relevant to medical applications and systematically compares the effects of unmodified and surface-modified CNC on dispersion, curing-related behaviour, and mechanical reinforcement at ultralow filler loadings.

In this study, both CNC and surface-modified CNC with enhanced hydrophobicity were incorporated into a soft elastomeric matrix. Although resins containing inherent hydroxyl groups may provide an alternative route in certain formulations, successful integration of CNC into hydrophobic resins generally requires surface modification of cellulose [31]. However, this approach may not be broadly applicable to other hydrophobic resin systems [32]. To address this limitation, 2-Hydroxyethyl acrylate (HEA) was introduced. In its polymerised form, HEA exhibits biocompatibility, low cytotoxicity, thermal stability and favourable cell compatibility, similar to poly(2-hydroxyethyl methacrylate), which is widely used in contact lens manufacturing [33]. Here, HEA was employed to reduce the hydrophobic mismatch of the resin system and to improve compatibility with unmodified CNC through its hydroxyl-functional character. Rather than acting as a crosslinking agent, HEA is more appropriately regarded as a hydroxyl-functional reactive monomer that may influence matrix polarity, local hydrogen-bonding interactions and interfacial compatibility within the resin system.

Therefore, in this study, HEA-based soft elastomeric resins containing varying concentrations of CNC and modified CNC were formulated and fabricated into specimens using VP-based 3D printing. Their physical and chemical properties were systematically evaluated to determine the optimal concentration range and to assess the reinforcing effects of CNC and modified CNC. Overall, this study aims to demonstrate the feasibility and functionality of incorporating CNC into elastomeric matrices and to establish a broadly applicable approach for integrating CNC into diverse resin systems.

2. Materials and methods

2.1. Materials and 3D printing

To prepare the soft elastomeric resin, a combination of oligomers and monomers was used. The base matrix consisted of 66.33% GR151 (Graphy Inc., Seoul, South Korea) and 13.27% HEA. GR151 consists of 65-70% urethane dimethacrylate oligomer, 5-10% dimethacrylate monomer, 30-35% acrylate monomer and less than 5% phosphine oxides and pigments. The monomer component included 8.16% 4-hydroxybutyl acrylate (4-HBA) and 12.24% trimethylolpropane formal acrylate (CTFA). CNC powder (Celluforce, Montreal, Canada) and acrylated CNC (ACNC) were prepared, with ACNC synthesised following the same modification procedure described previously [25]. The synthesis of ACNC was conducted by introducing polymerizable methacrylate groups onto the CNC surface, as illustrated

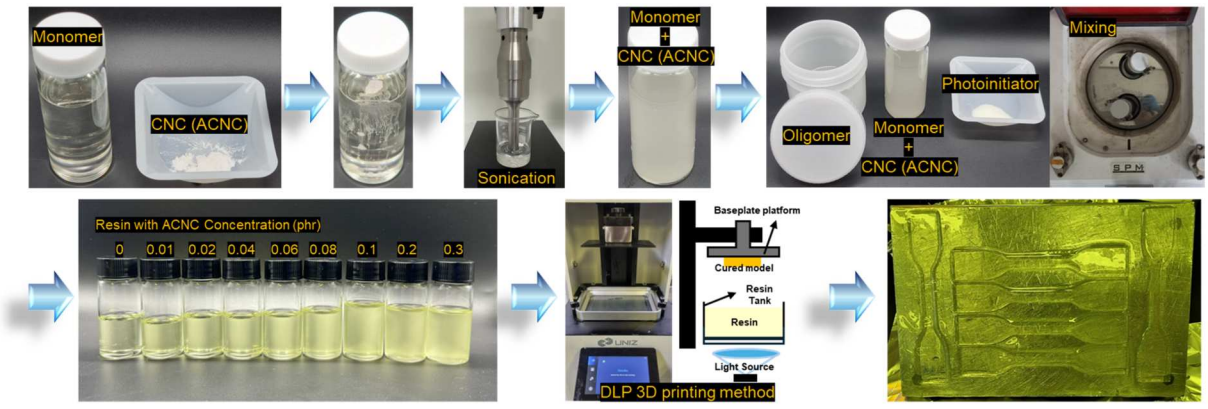

Figure 1. Schematic of the VP resin preparation, combining CNC/ACNC synthesis with the DLP 3D printing process.

in Figure 2(a). Initially, CNC was subjected to TEMPO-mediated oxidation. The oxidised CNC was then dispersed in deionised (DI) water at 60 °C, followed by the addition of methacrylic anhydride to initiate the methacrylation process. The reaction was maintained for 6 h to facilitate the substitution of hydroxyl (-OH) groups with methacrylate groups. After the reaction, the mixture was centrifuged to remove excess water. The resulting slurry was subsequently freeze-dried under vacuum at −80 °C to obtain the final ACNC product in powder form.

CNC and ACNC were incorporated into the base matrix at concentrations of 0.01, 0.02, 0.04, 0.06, 0.08, 0.1, 0.2 and 0.3 phr (Figure 1). For composite preparation, the required amount of CNC or ACNC was added to the monomer mixture at the target concentration. To disperse CNC or ACNC within the monomer mixture, sonication was performed using a VCX-750 sonicator (Sonics, USA) at 225 W for 1 h. The oligomers were then added in the specified ratios, followed by the addition of a photoinitiator. The final mixture was homogenised in a planetary mixer for 1 h. 3D printing was performed using a Uniz NBEE printer (Uniz, CA, USA) under the following conditions: laser power of 10 mW, exposure time of 1.1 s and layer thickness of 100 μm. Post-curing was conducted under a nitrogen atmosphere with 405 nm UV light at a power density of 34 J/min for 10 min.

2.2. Materials characterisation

To evaluate the effects of CNC and ACNC, tensile testing, transmission electron microscopy (TEM), Fourier-transform infrared spectroscopy (FTIR) and rheological measurements were conducted. Tensile tests were performed using a universal testing machine (Zwick Z010, ZwickRoell, Ulm, Germany) in accordance with ASTM D638 Type IV specifications. All concentrations, including the neat resin without CNC or ACNC, were tested with a minimum of 10 specimens per group to ensure reproducibility. Statistical analysis of the mechanical properties was performed using two-way analysis of variance (ANOVA), with material type (CNC and ACNC) and filler concentration as fixed factors. When significant main effects or interactions were identified, post hoc multiple comparisons were conducted using the Tukey-Kramer test to compare concentrations within each material group and to compare CNC and ACNC at the same concentration. A p-value < 0.05 was considered statistically significant. TEM imaging was conducted using a Tecnai G2 F30 S-Twin 300 kV microscope (FEI Company, USA). FTIR spectra were collected on a Nicolet iS50 spectrometer (Thermo Fisher Scientific, Waltham, MA, USA) over the wavenumber range of 4000–500 cm^{-1}, with a spectral resolution of 0.48 cm^{-1}. Rheological properties of the composites were measured on a rheometer (MCR 702e, Anton Paar Ltd., Austria) equipped with an 8 mm disposable parallel plate at 25 °C and a plate gap of 100 μm. Photo-rheological behaviour of the resin and photocurable composites was evaluated at a shear strain of 0.1% and a frequency of 1 Hz. A 405 nm UV LED (10 mW/cm^2) was used as the light source. Oscillation was applied for 60 s before UV exposure, which was maintained for 300 s. Shrinkage was recorded under a shear force of 0 N.

3. Results and discussion

3.1. Interaction mechanisms and long-term dispersion stability

Figure 2 presents a schematic illustration of the chemical interactions that likely influence the dispersion behaviour and network formation of CNC-reinforced GR-151 resin systems. As shown in Figure 2(a), sulfuric acid–derived CNC was subjected to TEMPO-mediated

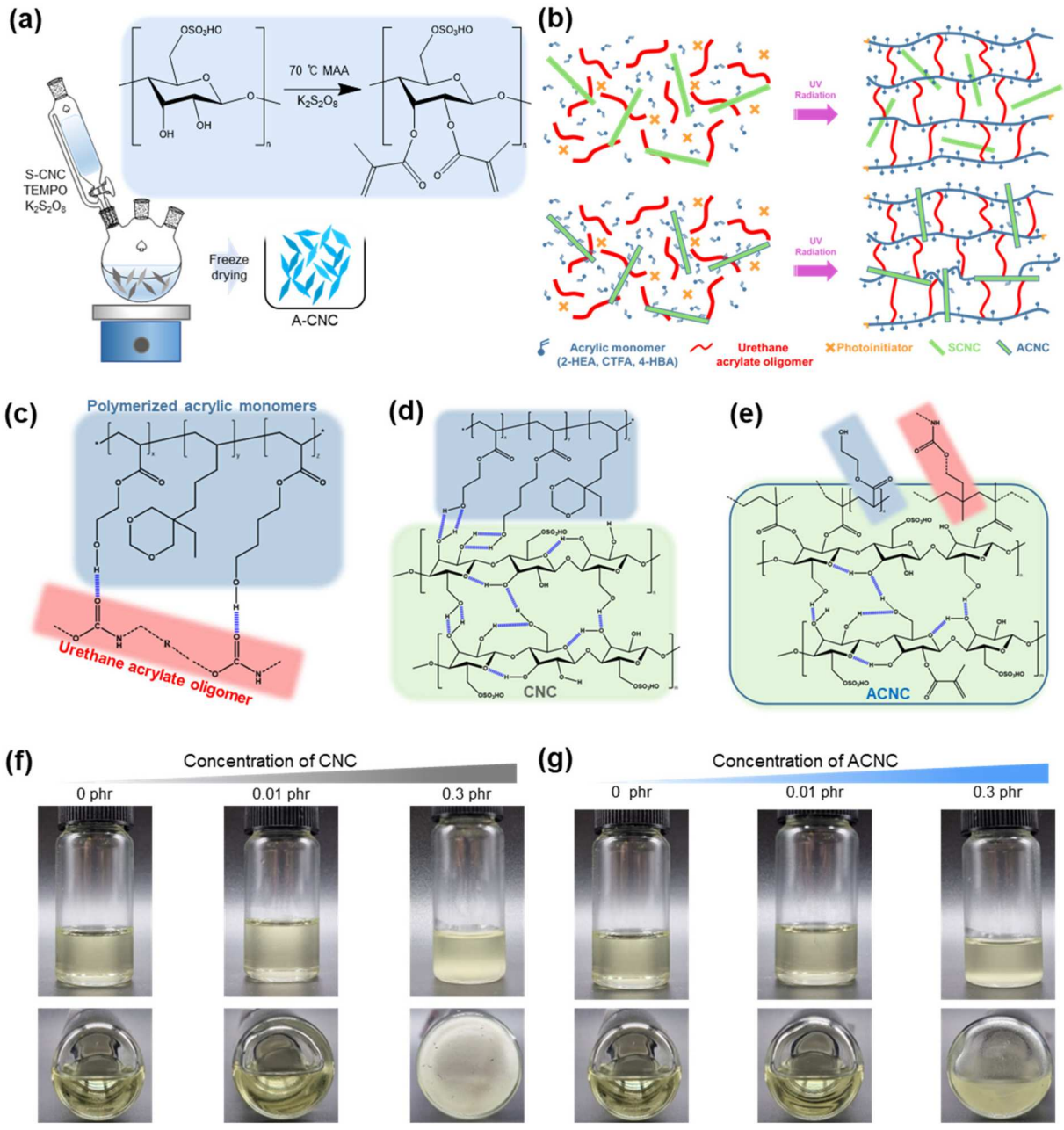

Figure 2. (a) Schematic illustration of the preparation of acrylated cellulose nanocrystals (ACNC) via TEMPO-mediated oxidation and subsequent methacrylation, followed by freeze-drying. (b) Chemical structure evolution of CNC during surface modification, showing the conversion of hydroxyl groups into polymerizable methacrylate functionalities. (c) Schematic representation of hydrogen bonding between urethane linkages in the urethane acrylate oligomer and terminal hydroxyl groups of acrylic monomers. (d) Hydrogen-bonding interactions between residual hydroxyl groups on unmodified sulfuric acid–derived CNC and hydroxyl groups of acrylic monomers. (e) Schematic illustration of covalent bond formation between methacrylate groups on ACNC and acrylic monomers or methacrylate-based oligomers through radical polymerisation. (f) Long-term dispersion stability of CNC in GR-151 resin at different concentrations after 1 year of storage. (g) Long-term dispersion stability of ACNC in GR-151 resin at corresponding concentrations after 1 year of storage.

oxidation followed by MAA, yielding ACNC with surface-grafted methacrylate groups. The corresponding chemical structure evolution is illustrated in Figure 2(b), highlighting the introduction of polymerizable vinyl functionalities onto the CNC surface. Prior to surface modification, intermolecular interactions within the resin matrix are expected to involve substantial hydrogen bonding. As depicted in Figure 2(c), urethane linkages present in the urethane acrylate oligomer form hydrogen bonds with hydroxyl groups at the termini of acrylic monomers, contributing to transient physical interactions within the uncured resin. Similarly,

unmodified CNC retains a high density of surface hydroxyl groups, which engage in extensive hydrogen bonding with hydroxyl-functional monomers, as schematically shown in Figure 2(d). While these interactions can initially assist dispersion, they also promote CNC-CNC agglomeration through strong interparticle hydrogen bonding. In contrast, surface acrylation fundamentally alters the role of CNC in the resin system. As illustrated in Figure 2(e), methacrylate groups on ACNC participate directly in radical polymerisation during UV irradiation, forming covalent bonds with acrylic monomers and methacrylate-based oligomers. This process likely changes the role of ACNC from a predominantly physically interacting filler to a more chemically integrated reinforcing phase that can participate in the photocured polymer network.

In addition to covalent crosslinking, hydroxyl-functional acrylate monomers, specifically HEA and 4-HBA, likely contribute to regulating interfacial interactions and local network homogeneity within the GR-151 resin system. The terminal hydroxyl groups present in HEA and 4-HBA participate in directional hydrogen bonding with multiple components of the resin matrix. First, these hydroxyl groups interact with urethane linkages within the urethane acrylate oligomer through N–H···O and O–H···O hydrogen bonds. These interactions may contribute to transient physical crosslinks that enhance chain entanglement prior to gelation and may moderate local chain mobility, thereby helping to create a more uniform curing environment during photopolymerization. The hydroxyl groups in HEA and 4-HBA may form hydrogen bonds with residual hydroxyl and sulfate ester groups on the CNC surface. In the case of unmodified CNC, these interactions increase local polarity and initially improve dispersion; however, excessive hydrogen bonding between CNC particles ultimately leads to agglomeration and phase separation over long-term storage. However, because HEA and 4-HBA were not independently varied in the present study, their individual contributions to dispersion and interfacial interactions could not be directly distinguished.

The impact of these distinct interaction mechanisms is evident in the long-term dispersion behaviour. Figures 2(f) and (g) compare the long-term dispersion stability of CNC and ACNC in the GR-151 resin at different filler loadings (0.01-0.2 phr) after 1 year of storage. As shown in Figure 2(f), CNC-containing resins exhibit concentration-dependent phase separation and sedimentation after 1 year of storage, reflecting poor interfacial compatibility and agglomeration driven by hydrogen bonding. In contrast, ACNC-containing resins maintain uniform dispersion across the same concentration range, even after prolonged storage (Figure 2(g)). This enhanced stability is more likely associated with improved interfacial compatibility and reduced agglomeration tendency after surface acrylation, which helped maintain a more uniform dispersion during prolonged storage. Overall, these observations suggest that surface acrylation of CNC modifies short-range intermolecular interactions and may influence both network development during photopolymerization and long-term dispersion stability in DLP-printable urethane acrylate resins.

3.2 Mechanical properties

Mechanical testing was first conducted to determine whether the incorporation of CNC or ACNC could enhance the tensile performance of the elastomeric resin and to identify the concentration range that provides the greatest reinforcement. The mechanical properties are shown in Figure 3. In this study, improvements in tensile strength and strain were affected by the addition of CNC and ACNC, depending on filler type and concentration. These findings are consistent with previous studies that reported enhancements in mechanical performance upon incorporation of CNC or modified CNC [20,22–25]. Li et al. reported that, in a PEGDA/DiGlyDA-based DLP system, the tensile strength reached 7.6 $\pm$ 0.3 MPa at 1 wt% CNC and the Young's modulus increased from 52.8 $\pm$ 1.4 MPa to 133.0 $\pm$ 4.0 MPa, with acceptable CNC dispersion primarily at loadings of approximately 1 wt% or less [24]. Rosa et al. also showed that CNC incorporation into a PEGDA/AESO SLA resin increased tensile strength by up to 59.1%, using filler contents in the range of 2.4 wt % [22]. More recently, Choi et al. reported that A-CNCs in a CTFA-based DLP resin exhibited the best tensile reinforcement at 0.1 wt%, while higher concentrations led to decreased performance due to increased light scattering and ineffective polymerisation [25].

In comparison, the present elastomeric resin system exhibited its greatest mechanical enhancement at 0.01 phr of both CNC and ACNC, indicating that meaningful reinforcement could be achieved at substantially lower filler loading in this specific soft VP-printable formulation (Figure 3). The elastic modulus was influenced by filler concentration, and its response differed between CNC and ACNC depending on concentration (Figure 3(c)). This enhancement suggests that the nanofillers not only act as reinforcing agents but may also influence the structural organisation of the surrounding polymer matrix, thereby improving the composite's overall elastic behaviour. These findings indicate that CNC and ACNC contribute to reinforcement through favourable

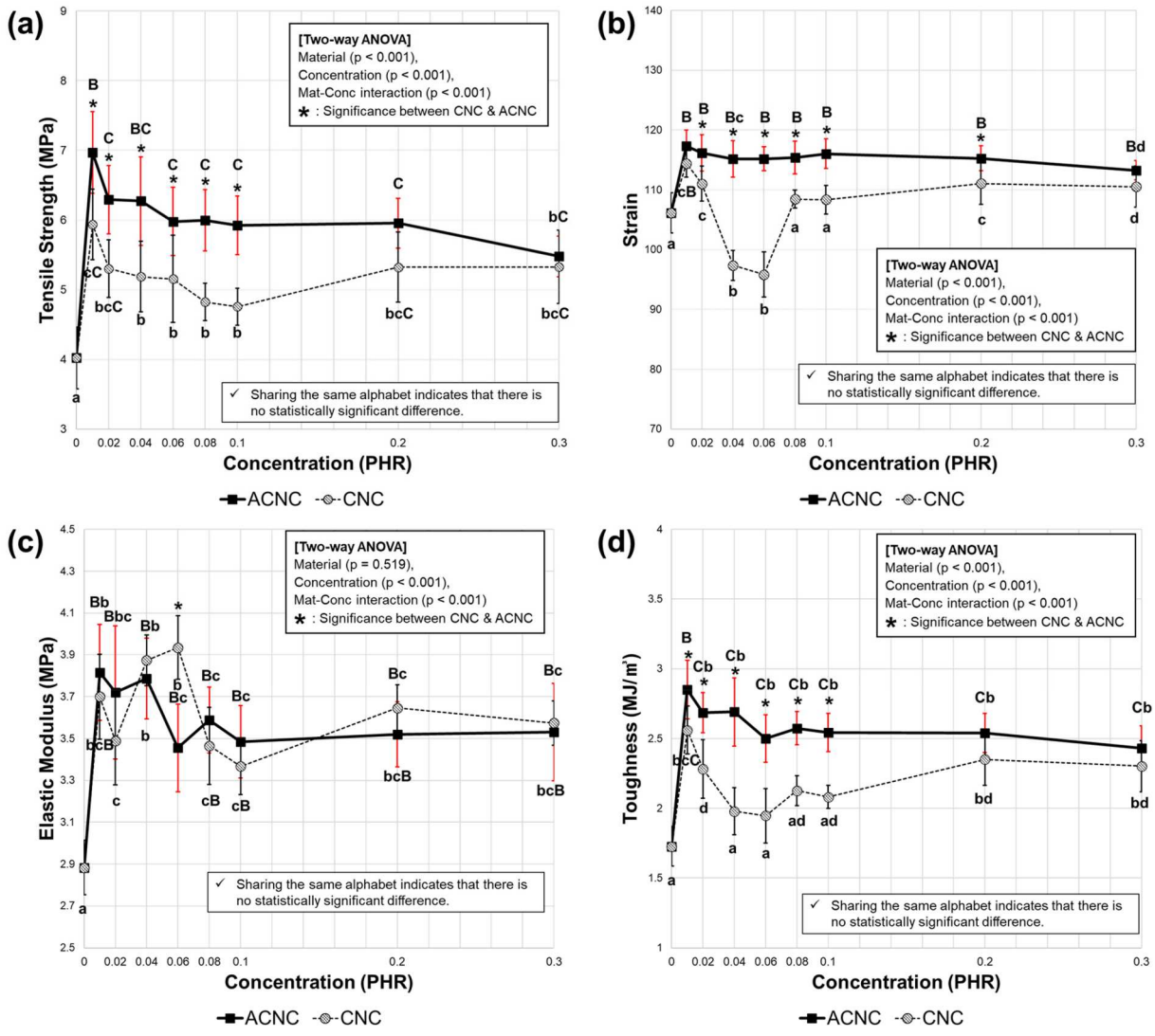

Figure 3. (a) Tensile strength, (b) strain, (c) elastic modulus, and (d) toughness as functions of CNC and ACNC concentration.

matrix–filler interactions. Toughness, defined as the area under the stress-strain curve, also exhibited an increasing trend with the addition of CNC and ACNC, aligning with the improvements observed in tensile strength and strain compared to the neat resin (Figure 3(d)). Although previous studies have identified optimal concentrations for CNC incorporation [19,23,24,28], the base matrix used in this study showed the greatest enhancement in mechanical properties with only 0.01 phr of CNC or ACNC, lower than concentrations reported in earlier work. These results suggest that, for the neat resin matrix employed here, the addition of only 0.01 phr of CNC or ACNC is sufficient to improve mechanical performance, indicating the potential for similar behaviour in other resin systems.

When comparing CNC and ACNC, ACNC generally resulted in greater improvements in tensile strength, strain and toughness, although the significance of the differences depended on the specific property and concentration. At a concentration of 0.01 phr, the tensile strength increased by 173% relative to the neat resin with ACNC, compared to a 117% increase with CNC (Figure 3(a)). At 0.01 phr, strain and toughness also showed significant improvement relative to the neat resin. Beyond 0.01 phr, ACNC also tended to show higher tensile strength, strain and toughness than CNC, although the statistical significance depended on the property and concentration. For strain, statistically significant differences between CNC and ACNC were observed at all concentrations (Figure 3(b)). For tensile strength and toughness, significant differences between CNC and ACNC were observed at most concentrations, with no significant difference at 0.3 phr. These results suggest that the methacrylate-functionalised ACNC achieved more effective matrix-filler interactions than unmodified CNC. This difference is likely associated

with polymerizable surface groups and improved interfacial compatibility rather than with a single bonding mechanism alone. The reduction in reinforcement observed for several mechanical properties at concentrations above 0.01 phr may be attributed to agglomeration. Despite the use of HEA or surface modification strategies such as ACNC functionalization, the inherently hydrophilic nature of CNC likely promotes self-agglomeration. With CNC, strain decreased at 0.04 and 0.06 phr, then increased again from 0.08 phr, which may be attributed to the higher absolute amount of CNC contributing to mechanical reinforcement despite agglomeration effects. In contrast, ACNC exhibited a different trend; due to its improved dispersion and stronger interfacial bonding with the matrix, no reduction in strain was observed at any concentration. Because the best mechanical performance was obtained at 0.01 phr, TEM analysis was next used to examine whether visible agglomeration increased at higher concentrations.

3.3 Nanostructure analysis

TEM analysis was performed to qualitatively examine whether the concentration-dependent mechanical trends could be associated with differences in filler distribution and visible agglomeration within the resin system. Figure 4 presents the TEM images. At a concentration of 0.01 phr, both CNC and ACNC showed a lower extent of visible agglomeration than at higher concentrations such as 0.06 and 0.3 phr, although small-scale agglomerates could still be observed. As the concentration increased, more pronounced particle-rich regions and larger agglomerates became evident, particularly at 0.3 phr. Therefore, the TEM images should not be interpreted as indicating a complete absence of agglomeration at low concentration, but rather as suggesting a relative increase in agglomeration tendency with increasing filler loading. These observations are consistent with the mechanical properties trend, in which the best performance was obtained at the lowest concentration, while higher concentrations showed a greater tendency toward agglomeration that may have reduced reinforcement efficiency. Because TEM provides localised images of selected regions, these observations should be regarded as qualitative evidence of relative agglomeration tendency rather than a definitive quantitative measurement of dispersion throughout the resin system. This interpretation is further supported by the long-term dispersion stability results, in which the CNC-containing formulations showed more pronounced phase separation and sedimentation over time, whereas the ACNC-containing formulations remained comparatively uniform (Figures 2(f) and (g)). Therefore, the dispersion interpretation in this study is based on the overall consistency among TEM observations, mechanical property trends and long-term dispersion stability, rather than on TEM evidence alone. While TEM provided qualitative information on filler distribution, FTIR was further used to examine whether ACNC also differed from CNC in terms of relative chemical functionality.

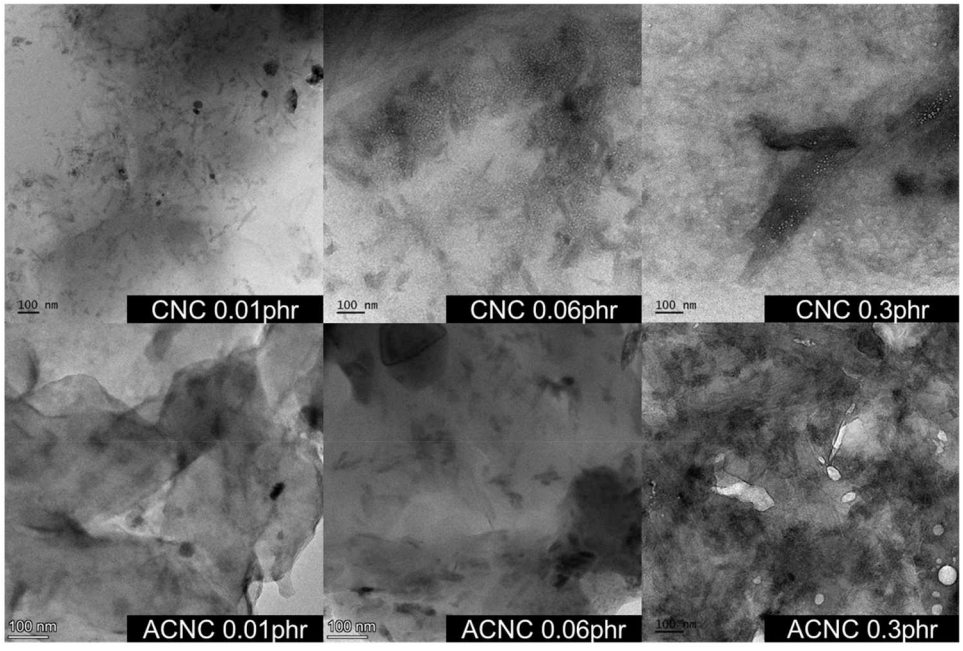

Figure 4. TEM images of CNC and ACNC at concentrations of 0.01, 0.06, and 0.3 phr.

3.4 FTIR analysis

FTIR analysis was performed to compare the relative chemical functionality of the cured neat, CNC-containing and ACNC-containing formulations and to assess whether ACNC introduced spectral features consistent with a more chemically favourable interface. The FTIR spectra shown in Figure 5 were collected from the cured formulations after photopolymerization. Because these spectra were not collected in a time-resolved manner, the FTIR results are interpreted here as supportive evidence of relative chemical functionality rather than direct proof of reaction progress or absolute bond formation. Peaks observed in the range of 1050–1150 cm^{-1} correspond to C–O–C stretching vibrations, characteristic of the base matrix backbone. Broad peaks between 3200 and 3600 cm^{-1} are attributed to –OH stretching vibrations, while peaks around 2900 cm^{-1} correspond to C–H stretching vibrations. C=O stretching vibrations were identified near 1700 cm^{-1}. Among these, the C=O stretching peak was most pronounced in the ACNC-con containing sample compared with both the neat resin and the CNC-containing sample. This increase is consistent with a greater relative contribution of carbonyl-containing functionalities in the ACNC system and suggests a more chemically favourable interface with the matrix, which may be associated with the improved mechanical properties. Moreover, the intensity of the C=O peak increased with higher ACNC concentrations (0.06 and 0.3 phr) relative to 0.01 phr, indicating a greater relative contribution of carbonyl-/ester-related functionality at increased loadings. To quantitatively evaluate this trend, the normalised FTIR peak intensity ratio ($I_{C=O}/I_{C-O-C}$) was calculated for each formulation (Table 1). At all investigated concentrations, the ACNC-containing resins exhibited higher values than the corresponding CNC-incorporated resins. This trend is consistent with the presence of acrylate/methacrylate-derived ester groups on the ACNC surface and suggests that ACNC provided a more chemically compatible interface with the resin matrix. Notably, the ratio increased with increasing ACNC concentration, indicating a greater relative contribution of carbonyl-related functionality at higher loadings. However, despite the increase in carbonyl-related functionality and interfacial chemical reactivity suggested by FTIR, mechanical performance did not improve beyond 0.01 phr, which is likely due to the negative effects of agglomeration. Therefore, while the FTIR results support enhanced interfacial reactivity in the ACNC system, the final mechanical performance was likely governed by a balance between chemical interaction and concentration-dependent agglomeration.

These findings suggest that at higher concentrations, agglomeration exerts a more dominant influence on mechanical behaviour than chemical bonding. Agglomeration likely disrupts effective stress transfer and reduces the reinforcing efficiency of ACNC. If future strategies can effectively suppress agglomeration at higher concentrations, the optimal concentration range for mechanical reinforcement may shift accordingly. To complement the post-cure FTIR results, photo-rheology was used to assess differences in early-stage network development during UV exposure.

3.4 Rheological analysis

Photo-rheological analysis was conducted to examine how CNC and ACNC affected early-stage viscoelastic evolution during UV exposure, thereby providing complementary information on network development before full post-curing. Changes in the storage modulus (G′) with CNC and ACNC incorporation are shown in Figures 6(a) and (b). Upon initiation of UV irradiation (at 60 s), G′ increased sharply as network formation progressed. The rheological data reflect the viscoelastic evolution of the formulations during early-stage UV exposure, but do not directly quantify double-bond conversion or final cure extent. Figure 6(e) compares the maximum storage modulus across different additive concentrations. Interestingly, the highest maximum storage modulus was observed for the neat resin and G′ decreased with increasing CNC or ACNC concentration, contrary to the trend observed in mechanical properties. The lower rheological response in the CNC-containing formulations may suggest that unmodified CNC affected early network development, although the present data do not allow a direct distinction between reduced conversion, delayed gelation, or other viscoelastic effects. This discrepancy may arise because the rheological analysis captures only the curing state during the early stage of the process, up to the point of 3D printing. In contrast, the tensile test specimens were evaluated after the final post-curing step. UV exposure during the rheological test was calibrated to match the energy intensity used during printing, resulting in only partial curing, approximately 60–70% of full network formation. Under these conditions, bonding between monomers may be more favourable, whereas reactions involving hydroxyl groups on CNC or methacrylate groups of ACNC are less likely to proceed, potentially affecting the curing process. As a result, the reinforcing effects of CNC and ACNC may not have been fully realised during rheological testing but became apparent after complete post-curing. The reduced modulus observed during rheological analysis

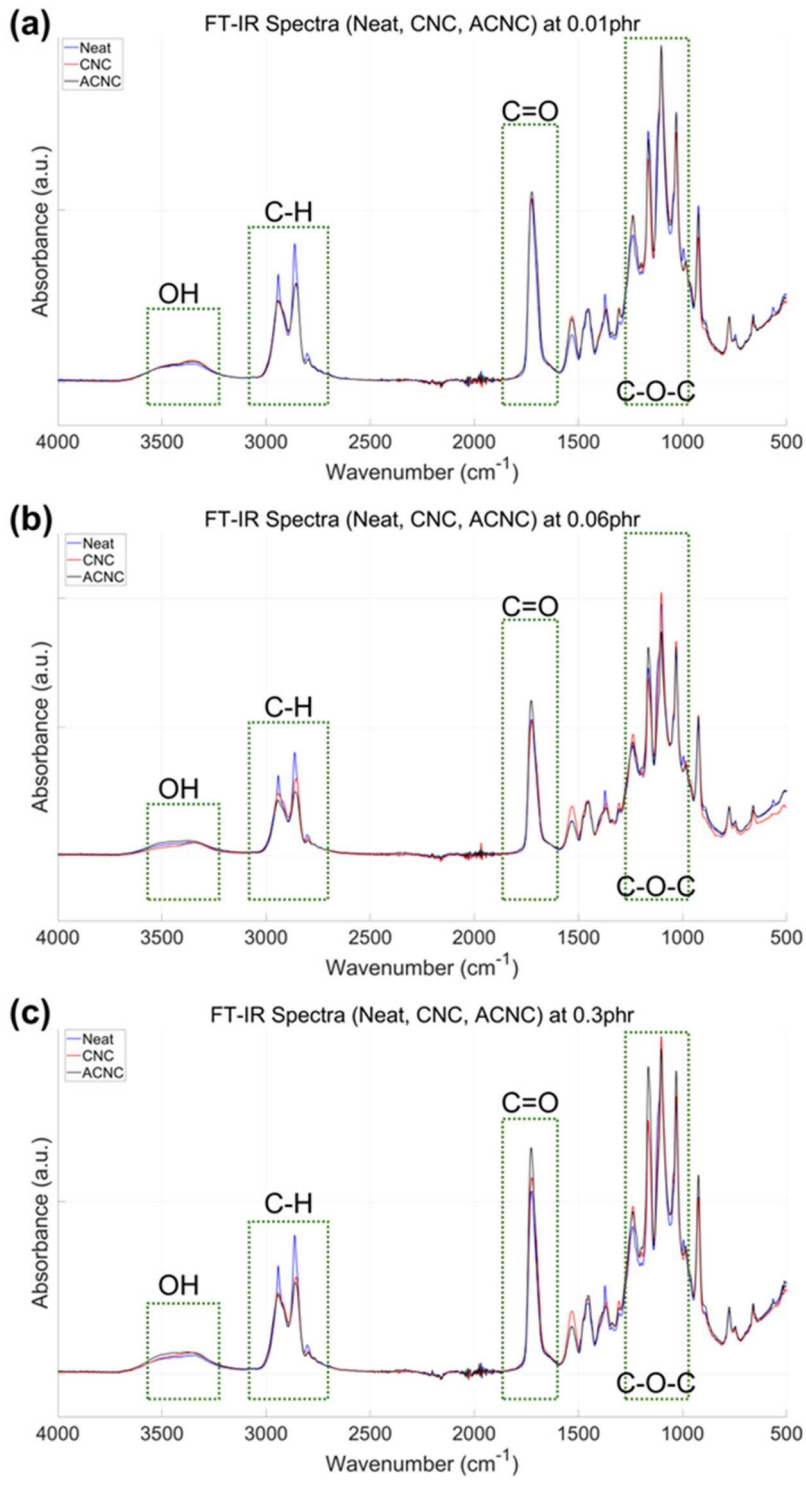

Figure 5. FTIR spectra of CNC- and ACNC-incorporated resins at concentrations of (a) 0.01, (b) 0.06, and (c) 0.3 phr. The highlighted regions indicate stretching vibrations corresponding to specific wavenumber ranges.

may also be attributed to the presence of unreacted monomers or oligomers surrounding CNC or ACNC particles, further limiting the development of a rigid network at this stage.

In the ACNC group, G′ values were comparable to those of the CNC group at concentrations ranging from 0.01 to 0.1 phr but were notably higher at 0.2 and 0.3 phr (Figure 6(e)). This suggests that the acrylate groups introduced onto the ACNC surface may have formed covalent bonds with the acrylate groups in the resin, resulting in a more robust and compact three-dimensional network that contributed to increased

Table 1. Normalised FTIR peak intensity ratios ($I_{C=O}/I_{C-O-C}$) for CNC- and ACNC-incorporated resins at varying concentrations.

FTIR Quantitative Ratio (C=O / C-O-C)		
0.3phr	Neat resin + CNC	0.94
	Neat resin + ACNC	1.68
0.06phr	Neat resin + CNC	0.80
	Neat raesin + ACNC	1.64
0.01phr	Neat resin + CNC	0.69
	Neat resin + ACNC	0.87

stiffness. In contrast, CNC interacted with the resin primarily through physical interactions, limiting its reinforcing effect on G′ even at higher concentrations. This distinction underscores the difference between ACNC, which may participate more directly in copolymerisation and network formation and CNC, which functions primarily as a passive filler. The relatively smaller decrease in storage modulus observed for ACNC at higher concentrations further suggests additional covalent bonds between its surface groups and surrounding monomers or oligomers. These rheological results are consistent with both mechanical testing and FTIR findings. Specifically, the increased intensity of the C=O stretching peak at higher ACNC concentrations aligns with the observed increase in storage modulus at 0.3 phr, suggesting more favourable network formation. Although mechanical performance did not peak at 0.3 phr due to agglomeration, the results suggest that ACNC may have formed more effective interfacial interactions at this concentration. With further mitigation of agglomeration, even greater improvements in mechanical properties may be achievable.

Figure 6(f) presents an enlarged view of the early-stage curing response at 0.01 phr. The faster early increase in G′ observed for the ACNC-containing formulation may indicate more rapid network buildup during the initial stage of photopolymerization, possibly due to improved interfacial compatibility and the presence of polymerizable surface groups. Upon UV irradiation, the ACNC-containing sample exhibited a rapid increase in G′, whereas the neat resin and CNC-containing sample showed nearly identical initial responses. Curing appeared to proceed more rapidly in the ACNC-containing formulation. This behaviour may be related to the presence of polymerizable surface groups and improved compatibility with the surrounding matrix, and may help explain the distinct curing response relative to the neat resin and CNC-containing systems. This result suggests that ACNC may interact more effectively with the resin. The rapid increase in G′ further supports the interpretation that acrylate groups on the ACNC surface facilitated chemical interactions with the resin, promoting early crosslink formation. Thus, although differences in maximum G′ were not prominent (Figure 6(e)), the accelerated early curing behaviour observed for ACNC at 0.01 phr (Figure 6(f)) is consistent with its improved mechanical performance. Because degree of conversion was not directly measured by RT-FTIR or DSC in the present study, the curing-related interpretations should be regarded as indirect and supportive rather than definitive. Collectively, these findings suggest that ACNC may have promoted more favourable early-stage network development than CNC, which is consistent with its improved mechanical performance after post-curing.

Figure 6(c) shows the time-dependent behaviour of the loss modulus (G″) for the resin containing CNC, where G″ increased after UV irradiation. This indicates a partial increase in the viscous component, but the overall influence of CNC particles on the viscoelastic behaviour of the resin was limited. In the absence of chemical bonding with the resin, CNC did not substantially affect energy dissipation during curing. By contrast, Figure 6(d) shows that G″ remained consistently higher in the presence of ACNC, suggesting that ACNC not only contributed to viscous resistance but also dispersed more uniformly within the resin. Through chemical bonding, ACNC may have enhanced both internal friction and energy dissipation of the polymer network, which can be related to improved mechanical properties. Although G′ values were similar for CNC- and ACNC-containing resins, G″ values were higher in the ACNC system, resulting in a lower loss tangent (G″/G′) for CNC. Since a lower loss tangent reflects more solid-like behaviour, this suggests that curing may have progressed further in the CNC-containing formulation than in the neat resin and further in the ACNC-containing formulation than in the CNC-containing formulation. These findings support the interpretation that the addition of CNC or ACNC altered the curing behaviour during the 3D printing process.

3.5 Applications

To evaluate whether the mechanically improved formulations also retained practical printability and application relevance, the optimised resin systems were tested in representative soft medical structures. As shown in Figure 7, the printability of each resin formulation was evaluated in practical applications. The soft elastomeric material was applied to patient-specific guides for kidney cancer resection and to cylindrical bile-duct stents. Both the neat resin and the resins containing CNC or ACNC at their previously identified optimal concentration of 0.01 phr were successfully printed without any printability issues (Figure 7(a)). Although steady-shear viscosity was not directly measured in the

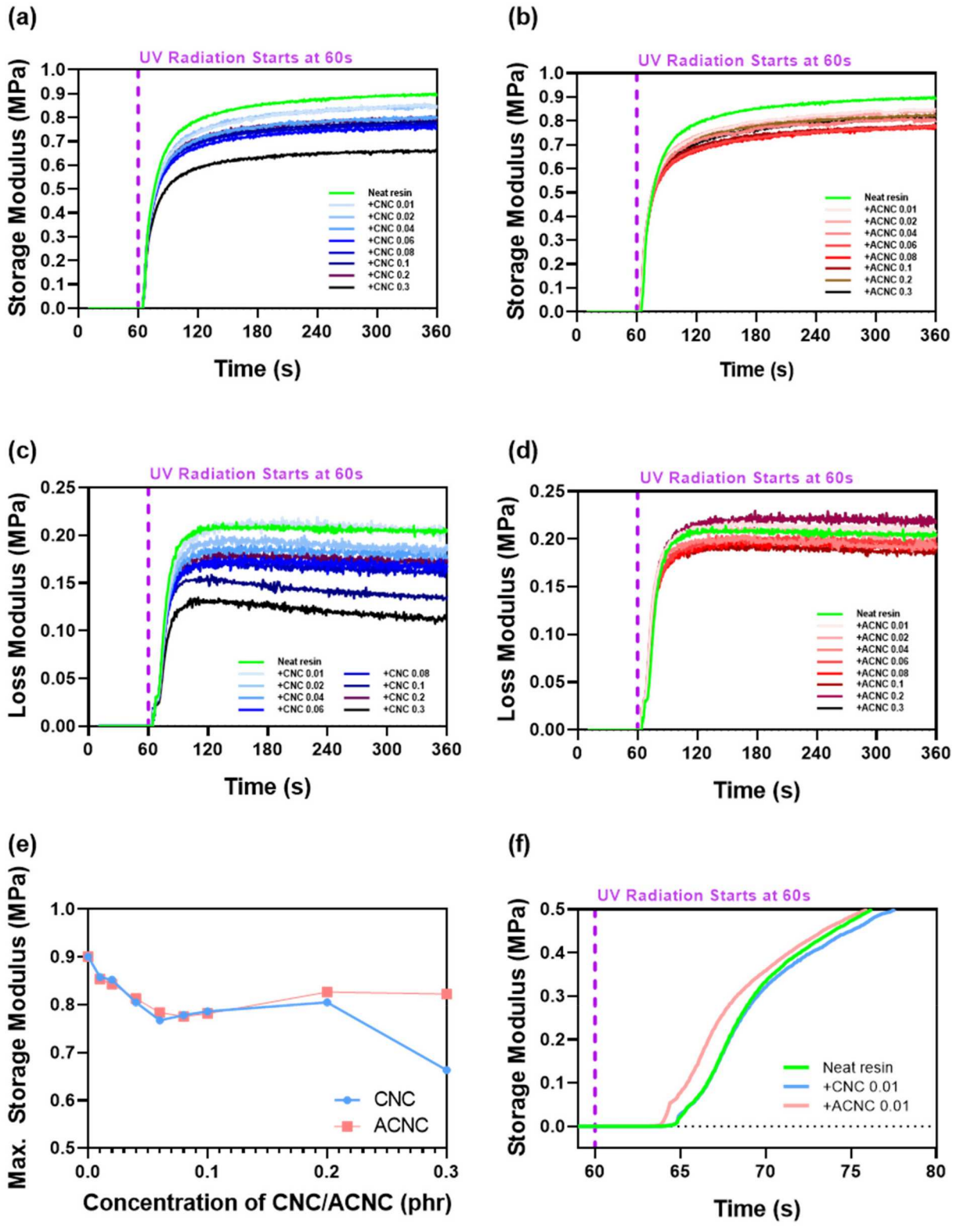

Figure 6. UV rheometer results for neat resin with varying concentrations of CNC/ACNC (0, 0.01, 0.02, 0.04, 0.06, 0.08, 0.1, 0.2, and 0.3 phr). UV irradiation begins at 60 s. Storage modulus (MPa) as a function of time (s) with (a) CNC and (b) ACNC. Loss modulus (MPa) with (c) CNC and (d) ACNC. (e) Maximum storage modulus at different CNC/ACNC concentrations. (f) Enlarged view of storage modulus at 0.01 phr CNC and ACNC near the onset of UV irradiation (60 s), highlighting the faster initial curing response of ACNC.

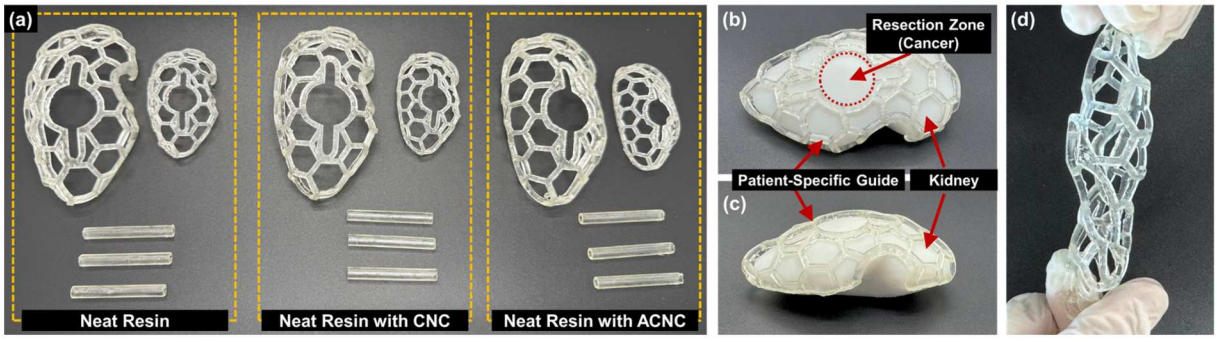

Figure 7. Patient-specific guides applied to the kidney and cylindrical stent structures for the bile duct. (a) Kidney patient-specific guides and bile duct stents fabricated using neat resin, resin with CNC, and resin with ACNC. (b) Frontal view of the kidney phantom model with the applied guide. (c) Lateral view of the kidney phantom model. (d) Deformation behaviour under torsion, demonstrating soft elastic material properties.

present study, the successful printing of the CNC- and ACNC-containing formulations at 0.01 phr indicates that filler addition at the optimal concentration did not adversely affect practical printability. Sedimentation during printing was not directly monitored. However, the absence of obvious printing defects suggests that any in-process instability was not severe enough to compromise fabrication under the present conditions. A kidney phantom model was fabricated, and the patient-specific guide (designed by Anymedi Inc.) was applied, as demonstrated in Figures 7(b) and (c). The guide exhibited an excellent fit to the kidney model and enabled clear identification of the resection zone. Furthermore, even under torsion, as shown in Figure 7(d), the structure did not fracture but maintained its integrity while deforming. These results indicate that the material, while preserving its original shape, is suitable for applications requiring contact with relatively soft organs such as the kidney or passage through narrow anatomical pathways. The ability to satisfy these application requirements while also providing favourable mechanical performance highlights the improved durability of the material.

4. Conclusions

In 3D printing for medical applications, there is a growing demand for soft, high-performance and printable material systems. In this study, CNC and ACNC were incorporated into an elastomeric photocurable resin to evaluate their effects on mechanical reinforcement, dispersion behaviour and printability.

The incorporation of both CNC and ACNC improved tensile strength, strain, elastic modulus and toughness relative to the neat resin. ACNC showed the greatest overall enhancement, likely owing to its surface acrylate functionalities, which may have improved compatibility with the resin matrix and enabled more effective matrix-filler interactions than unmodified CNC. The best mechanical performance was obtained at 0.01 phr.

Taken together, the results suggest that the optimal mechanical response at 0.01 phr arose from a balance between beneficial interfacial interactions and the onset of concentration-dependent agglomeration. FTIR and photo-rheological trends were consistent with more favourable interfacial behaviour in the ACNC-containing system, whereas TEM indicated that visible agglomeration became more pronounced at higher loadings. Thus, increasing filler concentration did not lead to continued mechanical improvement, likely because agglomeration progressively reduced reinforcement efficiency.

In addition, the successful fabrication of the CNC- and ACNC-containing formulations at 0.01 phr demonstrated that reinforcement could be achieved without compromising practical printability under the present printing conditions. These findings support the feasibility of incorporating CNC-based fillers into the specific soft elastomeric VP-printable resin platform investigated here.

Because the present study examined a single resin formulation and degree of conversion, steady-shear viscosity and optical transmittance were not directly quantified, the mechanistic interpretations should be regarded as supportive rather than definitive. Future work should therefore focus on optimising formulation and processing conditions, directly characterising curing conversion and flow behaviour and evaluating whether similar trends are maintained in other soft photocurable resin systems.

Acknowlegements

This paper was supported by Korea Evaluation Institute of Industrial Technology (KEIT) grant funded by the Korea Government (MOTIE) (20023781). This work was supported by

the InnoCORE program of the Ministry of Science and ICT (N10250154). The authors thank Jinho Hyun of Seoul National University for providing the modified cellulose nanocrystals. The authors thank Anymedi Inc. for providing kidney patient-specific guide design.

Author contributions

CRediT: **Wonhee Lee:** Conceptualization, Data curation, Formal analysis, Investigation, Methodology, Visualization, Writing – original draft, Writing – review & editing; **Eui-Hyuk Kim:** Investigation; **Tim Kuehnel:** Investigation; **Jinhong Min:** Investigation, Resources; **Jiho Lee:** Visualization; **Hoon Kim:** Conceptualization, Supervision, Writing – review & editing; **Yong-Jin Yoon:** Conceptualization, Supervision, Writing – review & editing.

Disclosure statement

No potential conflict of interest was reported by the author(s).

Funding

This work was supported by Korea Evaluation Institute of Industrial Technology: [Grant Number 20023781]; Ministry of Science and ICT, South Korea: [Grant Number N10250154].

Data availability statement

The data that support the findings of this study are openly available in Mendeley Data at [doi: 10.17632/5ck87d2f5g.1], under the [CC BY 4.0 license].

ORCID

Wonhee Lee http://orcid.org/0000-0001-7972-9969
Jinhong Min http://orcid.org/0000-0001-8178-7439
Jiho Lee http://orcid.org/0000-0003-2408-2808
Hoon Kim http://orcid.org/0000-0002-4447-4553
Yong-Jin Yoon http://orcid.org/0000-0002-3885-4947

References

[1] ISO/ASTM. ISO/ASTM 52900:2021(E), additive manufacturing — general principles — fundamentals and vocabulary. Geneva: International Organization for Standardization; 2021.
[2] Jandyal A, Chaturvedi I, Wazir I, et al. 3D printing – A review of processes, materials and applications in industry 4.0. Sustain Oper Comput. 2022;3:33–42. doi:10.1016/j.susoc.2021.09.004
[3] Tabassum T, Ahmad Mir A. A review of 3d printing technology-the future of sustainable construction. Mater Today Proc. 2023;93:408–414. https://doi.org/10.1016/j.matpr.2023.08.013.
[4] Kim GB, Lee S, Kim H, et al. Three-dimensional printing: basic principles and applications in medicine and radiology. Korean J Radiol. 2016;17(2):182–197. doi:10.3348/kjr.2016.17.2.182
[5] Bozkurt Y, Karayel E. 3D printing technology; methods, biomedical applications, future opportunities and trends. J Mater Res Technol. 2021;14:1430–1450. doi:10.1016/j.jmrt.2021.07.050
[6] Mamo HB, Adamiak M, Kunwar A. 3D printed biomedical devices and their applications: a review on state-of-the-art technologies, existing challenges, and future perspectives. J Mech Behav Biomed Mater. 2023;143:105930. doi:10.1016/j.jmbbm.2023.105930
[7] Dikova TD, Dzhendov DA, Ivanov D, et al. Dimensional accuracy and surface roughness of polymeric dental bridges produced by different 3D printing processes. Arch Mater Sci Eng. 2018;94(94):65–75. doi:10.5604/01.3001.0012.8660
[8] Kim T, Lee S, Kim GB, et al. Accuracy of a simplified 3D-printed implant surgical guide. J Prosthet Dent. 2020;124(2):195–201.e2. doi:10.1016/j.prosdent.2019.06.006
[9] Lee W, Yu W, Lee HY, et al. Evaluation of the baseplate position and screws in reverse total shoulder arthroplasty using 3D printed patient-specific instrumentation. J Orthop Res. 2025;43(10):1695–1704. doi:10.1002/jor.70023
[10] Ock J, Kim T, On S, et al. Utilizing patient-specific 3D printed kidney surgical guide with realistic phantom for partial nephrectomy. Sci Rep. 2023;13(1):15531. doi:10.1038/s41598-023-42866-9
[11] Ornaghi HL, Monticeli FM, Agnol LD. A review on polymers for biomedical applications on hard and soft tissues and prosthetic limbs. Polymers (Basel). 2023;15(19):4034. doi:10.3390/polym15194034
[12] Duran MM, Moro G, Zhang Y, et al. 3D printing of silicone and polyurethane elastomers for medical device application: a review. Adv Ind Manuf Eng. 2023;7:100125. doi:10.1016/j.aime.2023.100125
[13] Patel DK, Sakhaei AH, Layani M, et al. Highly stretchable and UV curable elastomers for digital light processing based 3D printing. Adv Mater. 2017;29(15). doi:10.1002/adma.201606000
[14] Kim S, Lee J, Han H. Synthesis of UV curable, highly stretchable, transparent poly(urethane-acrylate) elastomer and applications toward next generation technology. Macromol Res. 2020;28(10):896–902. doi:10.1007/s13233-020-8125-x
[15] Du K, Basuki J, Glattauer V, et al. Digital light processing 3D printing of PDMS-based soft and elastic materials with tunable mechanical properties. ACS Appl Polym Mater. 2021;3:3049–3059. doi:10.1021/acsapm.1c00260
[16] Huang X, Peng S, Zheng L, et al. 3D printing of high viscosity UV-curable resin for highly stretchable and resilient elastomer. Adv Mater. 2023;35(49). doi:10.1002/adma.202304430
[17] Mariano M, El Kissi N, Dufresne A. Cellulose nanocrystals and related nanocomposites: review of some properties and challenges. J Polym Sci B Polym Phys. 2014;52(12):791–806. doi:10.1002/polb.23490
[18] Ji A, Zhang S, Bhagia S, et al. 3D printing of biomass-derived composites: application and characterization approaches. RSC Adv. 2020;10(37):21698–21723. doi:10.1039/d0ra03620j
[19] Palaganas NB, Mangadlao JD, De Leon ACC, et al. 3D printing of photocurable cellulose nanocrystal composite for fabrication of complex architectures via stereolithography. ACS Appl Mater Interfaces. 2017;9(39):34314–34324. doi:10.1021/acsami.7b09223

[20] Abidnejad R, Mousapour M, Meinander K, et al. Digital light processing 3D printing: harnessing micro- and nanocellulose for advanced biocomposites. Int J Biol Macromol. 2025;321:146045. doi:10.1016/j.ijbiomac.2025.146045

[21] Kargarzadeh H, Sheltami RM, Ahmad I, et al. Cellulose nanocrystal: a promising toughening agent for unsaturated polyester nanocomposite. Polymer (Guildf). 2015;56:346–357. doi:10.1016/j.polymer.2014.11.054

[22] Palucci Rosa R, Rosace G, Arrigo R, et al. Preparation and characterization of 3D-printed biobased composites containing micro-or nanocrystalline cellulose. Polymers (Basel). 2022;14(9):1886. doi:10.3390/polym14091886

[23] Maturi M, Spanu C, Fernández-Delgado N, et al. Fatty acid – functionalized cellulose nanocomposites for vat photopolymerization. Addit Manuf. 2023;61:103342. doi:10.1016/j.addma.2022.103342

[24] Li VCF, Kuang X, Mulyadi A, et al. 3D printed cellulose nanocrystal composites through digital light processing. Cellulose. 2019;26(6):3973–3985. doi:10.1007/s10570-019-02353-9

[25] Choi J, Thakur D, Min J, et al. Incorporation of acrylated cellulose nanocrystals into photocurable resin for high-fidelity printing of transparent 3D structures. J Manuf Process. 2025;139:1–11. doi:10.1016/j.jmapro.2025.02.023

[26] Wong LY, Ganguly S, Tang X. 3D vat photopolymerization printing of hydrophilic silicone-based microfluidic devices and the effect of cellulose nanocrystals as additives for improved printing accuracy. Addit Manuf. 2024;86:104177. doi:10.1016/j.addma.2024.104177

[27] Ding Y, Bai Y, Wang T, et al. Strong and tough liquid crystal elastomers reinforced by cellulose nanocrystals for energy absorption. Polym Compos. 2026;47(2):1632–1643. doi:10.1002/pc.70241

[28] Palaganas NB, Palaganas JO, Doroteo SHZ, et al. Covalently functionalized cellulose nanocrystal-reinforced photocurable thermosetting elastomer for 3D printing application. Addit Manuf. 2023;61:103295. doi:10.1016/j.addma.2022.103295

[29] Wang Q, Liu X, Qiang Z, et al. Cellulose nanocrystal enhanced, high dielectric 3D printing composite resin for energy applications. Compos Sci Technol. 2022;227:109601. doi:10.1016/j.compscitech.2022.109601

[30] Chu B, Cui X, Dong X, et al. SLA printing of shape memory bio-based composites consisting of soybean oil and cellulose nanocrystals. Virtual Phys Prototyp. 2024;19(1):e2401933. doi:10.1080/17452759.2024.2401933

[31] Mohan D, Teong ZK, Bakir AN, et al. Extending cellulose-based polymers application in additive manufacturing technology: a review of recent approaches. Polymers (Basel). 2020;12(9):1876. doi:10.3390/POLYM12091876

[32] Kumar S, Hofmann M, Steinmann B, et al. Reinforcement of stereolithographic resins for rapid prototyping with cellulose nanocrystals. ACS Appl Mater Interfaces. 2012;4(10):5399–5407. doi:10.1021/am301321v

[33] Hoogenboom R, Popescu D, Steinhauer W, et al. Nitroxide-mediated copolymerization of 2-hydroxyethyl acrylate and 2-hydroxypropyl acrylate: copolymerization kinetics and thermoresponsive properties. Macromol Rapid Commun. 2009;30(23):2042–2048. doi:10.1002/marc.200900507